American Mineralogist, Volume 99, pages 198–205, 2014

Monipite, MoNiP, a new phosphide mineral in a Ca-Al-rich inclusion from the Allende meteorite

Chi Ma*, John R. Beckett and George R. Rossman

Division of Geological and Planetary Sciences, California Institute of Technology, Pasadena, California 91125, U.S.A.

Abstract

Monipite (IMA 2007-033), MoNiP, is a new phosphide mineral that occurs as one 1 × 2 μm crystal in a Type B1 Ca-Al-rich inclusion (CAI) ACM-2 from the Allende CV3 carbonaceous chondrite. It has an empirical formula of $(Mo_{0.84}Fe_{0.06}Co_{0.04}Rh_{0.03})(Ni_{0.89}Ru_{0.09})P$, and a $P\bar{6}2m$ Fe_2P type structure with a = 5.861, c = 3.704 Å, V = 110.19 Å^3, and Z = 3. The calculated density using our measured composition is 8.27 g/cm^3, making monipite the densest known mineral phosphide. Monipite probably either crystallized from an immiscible P-rich melt that had exsolved from an Fe-Ni-enriched alloy melt that formed during melting of the host CAI or it exsolved from a solidified alloy. Most of the original phosphide in the type occurrence was later altered to apatite and Mo-oxides, leaving only a small residual grain. Monipite occurs within an opaque assemblage included in melilite that contains kamiokite ($Fe_2Mo_3O_8$), tugarinovite (MoO_2), and a Nb-rich oxide [$(Nb,V,Fe)O_2$], none of which has previously been reported in meteorites, together with apatite, awaruite (Ni_2Fe), and vanadian magnetite.

Keywords: Monipite, MoNiP, new mineral, tugarinovite, kamiokite, Allende, carbonaceous chondrites, EBSD, Ca-Al-rich inclusions

Introduction

Schreibersite and barringerite are well-known phosphides from iron and stony iron meteorites, but phosphides are rare in carbonaceous chondrites, very rare in CV3 chondrites (Jambor et al. 2000; Riches et al. 2010) and, to our knowledge, have not been reported at all in Allende. It is phosphates, not phosphides, that are typically observed in carbonaceous chondrites (e.g., Armstrong et al. 1985, 1987). The reason for this is straightforward. Conditions during metasomatism of Allende and similar meteorites were quite oxidizing such that phosphates became the stable P-bearing minerals. Exposed phosphides were generally destroyed but, here, we describe monipite, a rare phosphide survivor of the metasomatism of the Allende CV3 carbonaceous chondrite, and explore its origin and evolution. Preliminary results are given in Ma et al. (2009a).

The ternary phosphide MoNiP is a well-known synthetic material because of its potential use as a hydrodesulfurization catalyst during petroleum refining (e.g., Sun et al. 2004; Nagai et al. 2005) and because it is a superconductor with a—for a phosphide—high critical temperature (Shirotani et al. 2000). Monipite, natural MoNiP, is the first phosphide mineral with molybdenum as a major constituent and the second mineral with the barringerite Fe_2P type structure. It is also the first reported occurrence of a phosphide in Allende.

Mineral name and type material

The new mineral and its name have been approved by the Commission on New Minerals, Nomenclature and Classification of the International Mineralogical Association (IMA 2007-033). Monipite is the Mo-,Ni-dominant analog of barringerite, Fe_2P. The mineral name monipite is derived from the three major elemental constituents (molybdenum, nickel, and phosphorus). A polished thin section, prepared from a 1 cm diameter Allende fragment (Caltech Meteorite Collection No. Allende-12A) contains the holotype material of monipite within a CAI. This section was deposited in the Smithsonian Institution's National Museum of Natural History with the catalog number USNM 7554. Type allendeite, grossmanite, hexamolybdenum, and hibonite-(Fe), which were described by Ma and Rossman (2009b), Ma et al. (2009b), and Ma (2010), are also present in this section.

Appearance, physical, and optical properties

The holotype grain of monipite is 1 × 2 μm in the plane of the section (see Figs. 1 and 2; see Fig. 1 for a larger-scale petrographic context). It is in contact with apatite, tugarinovite (MoO_2), and a Ru-Mo-Ni enriched alloy. The grain is opaque and non-cathodoluminescent under the electron beam in an SEM. Luster, streak, hardness, cleavage, fracture, and details of the optical properties were not determined because of the small grain size. The calculated density using our measured composition and the structure and cell parameters of synthetic MoNiP from Guérin and Sergent (1977) is 8.27 g/cm^3 (see below).

Chemical composition

Backscatter electron (BSE) images were obtained using a ZEISS 1550VP field emission SEM and a JEOL 8200 electron microprobe with solid-state BSE detectors. Quantitative elemental micro-analyses were conducted with the JEOL 8200 electron microprobe operated at 15 kV and 5 nA in focused beam mode. Standards for the analysis of monipite were Mo (Mo$L\alpha$), Ni (Ni$K\alpha$), GaP (P$K\alpha$), Ru (Ru$L\alpha$), Rh (Rh$L\alpha$), Fe (Fe$K\alpha$), and Co

* E-mail: chi@gps.caltech.edu

0003-004X/14/0001–198$05.00/DOI: http://dx.doi.org/10.2138/am.2014.4512

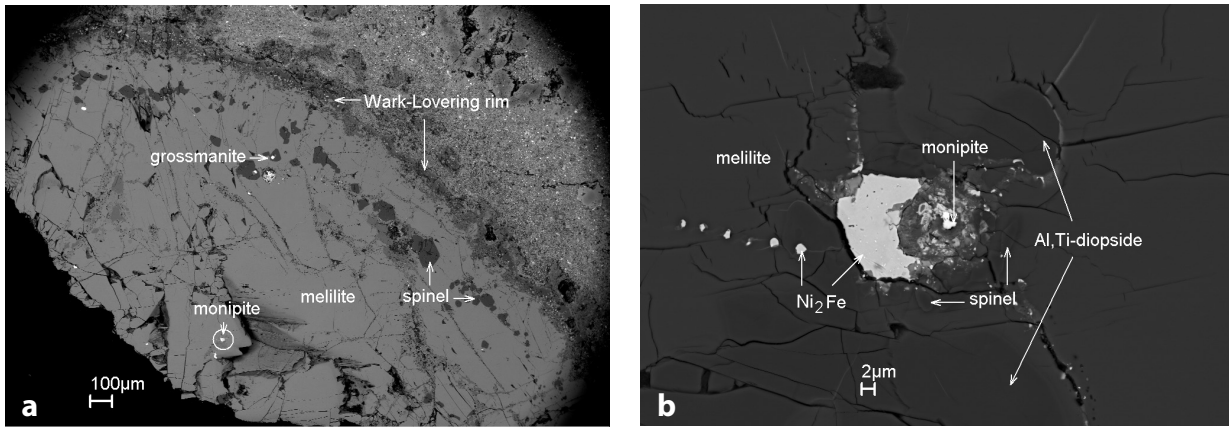

FIGURE 1. (**a**) Backscatter electron (BSE) image of CAI host of the monipite-bearing phase assemblage in USNM 7554. The location of monipite is enclosed by a circle. (**b**) BSE image showing the region where the monipite micro-crystal and its associated phases are located. The opaque assemblage is bounded on one side mostly by Al,Ti-diopside and spinel and on the other mostly by melilite.

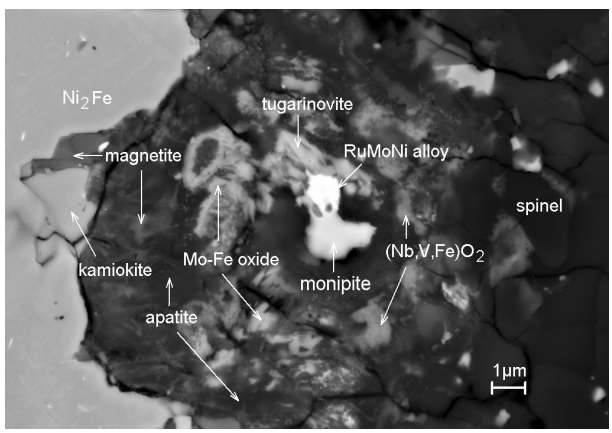

FIGURE 2. Enlarged BSE image showing the monipite micro-crystal and its associated phases.

(Co$K\alpha$). Analyses were processed using the CITZAF correction procedure (Armstrong 1995). An Oxford INCA X-ray energy-dispersive spectrometer (EDS) on the ZEISS SEM was also used for elemental analysis. These data were processed using the XPP correction procedure (Pouchou and Pichoir 1991).

Compositions of phases from the host inclusion, oxides, and apatite from the opaque assemblage containing monipite are given in Table 1. In Table 2, we give compositions of alloys and monipite. Opaque assemblages are complex, multi-phase objects that occur in carbonaceous chondrites [see Blum et al. (1989) for a general description] and are generally thought to be oxidation/sulfidation products of alloys or alloy-rich phase assemblages. Some of the compositions reported in Table 1 reflect mixtures of the target phase with nearby or surrounding phases. Such data are the best we can do at present and are given to maximize information about the phase assemblages in the vicinity of monipite.

The empirical formula of type monipite by EPMA is $(Mo_{0.84}Fe_{0.06}Co_{0.04}Rh_{0.03})(Ni_{0.89}Ru_{0.09})P$. The end-member formula is MoNiP, which requires Mo 51.68, Ni 31.63, P 16.69, total 100.00 wt%.

CRYSTALLOGRAPHY

Single-crystal electron backscatter diffraction (EBSD) analyses at a sub-micrometer scale were performed using an HKL EBSD system on the ZEISS 1550VP scanning electron microscope operated at 20 kV and 9 nA in focused beam mode with a 70° tilted stage and in a variable pressure mode (25 Pa). The EBSD system was calibrated using a single-crystal silicon standard. The structure of monipite was determined and cell constants obtained by matching the observed EBSD pattern against the structures of synthetic phases in the Mo-Ni-P system (Guérin and Sergent 1977; Shirotani et al. 2000). The $P\bar{6}2m$ MoNiP structure (Guérin and Sergent 1977) yields the lowest mean angular deviation (MAD) with MAD values of 0.3~0.7° (Fig. 3). Alternative candidate structures had much higher MAD values (~1.0°).

From the cell parameters of MoNiP (Guérin and Sergent 1977), the cell parameters for monipite are $a = 5.861$, $c = 3.704$ Å, $V = 110.19$ Å^3, $Z = 3$. Note that errors are not given for these cell parameters because they are taken directly from the data of the matching synthetic phase. Accepting these parameters for monipite, the calculated density using our measured composition is then 8.27 g/cm^3, which is the highest known density for a natural phosphide. Monipite assumes a Fe_2P type structure constructed from successive layers of Ni + P and Mo + P with Ni and Mo in tetrahedral and square-pyramidal coordination, respectively (Guérin and Sergent 1977; Shirotani et al. 2000).

The X-ray powder-diffraction data (in angstroms for Cu$K\alpha_1$) are taken from PDF 71-0202. The strongest calculated lines are [d in angstroms, intensity, I, scaled to 100 for the most intense peak, (hkl)] [2.298, 100, (111)], [1.918, 73, (210)], [2.094, 69, (201)], [1.852, 24, (002)], [1.408, 20, (310)], [1.316, 18, (311)], [1.332, 17, (212)], and [1.111, 14, (321)].

Raman micro-analysis of monipite was carried out using a Renishaw M1000 micro-Raman spectrometer system and a 514.5 nm laser using methods described in Ma and Rossman (2008, 2009a). The Raman spectrum for monipite (Fig. 4), shows Raman features at 280, 350, and 430 cm^{-1}.

TABLE 1. Oxides, phosphates, and silicates within and around or near the monipite-bearing phase assemblage

Phase	Al,Ti-diopside	melilite	spinel	kamiokite	V-rich magnetite	$(Nb,V,Fe)O_2$[a]	apatite[b]	Tugarinovite[c]	Mo-Fe-oxide[d]
Section	USNM 7554	USNM 7554	USNM 7554	USNM 7554	USNM 7554	USNM 7554	USNM 7554	USNM 7554	USNM 7554
Type	EPMA[e]	EPMA	SEM-EDS[f]	SEM-EDS	SEM-EDS	SEM-EDS	SEM-EDS	SEM-EDS	SEM-EDS
No. analyses	7	6	1	1	1	1	1	1	1
Na_2O	0.01(1)	0.02(1)	n.d.	n.d.	n.d.	n.d.	n.d.	n.d.	n.d.
MgO	8.0(6)[e]	2.84(3)	17.4(3)[f]	2.5(1)	1.1(1)	1.2(2)	1.9(2)	0.9(3)	0.8(3)
Al_2O_3	20.5(9)	29.4(1)	63.7(6)	n.d.	3.0(2)	1.2(2)	n.d.	n.d.	n.d.
SiO_2	38(1)	26.5(1)	n.d.	n.d.	1.1(2)	n.d.	n.d.	n.d.	n.d.
P_2O_5	n.d.[g]	n.d.	n.d.	n.d.	n.d.	11.6(6)	41.9(9)	3.1(6)	22(1)
CaO	25.5(2)	41.9(2)	n.d.	0.81(1)	1.7(1)	20.0(5)	47.8(8)	4.1(4)	28.8(9)
TiO_2	7(1)	0.01(1)	n.d.	n.d.	n.d.	n.d.	n.d.	n.d.	n.d.
V_2O_3	0.7(3)	0.01(1)	2.6(2)	n.d.	13.4(3)	13.1(6)	n.d.	n.d.	n.d.
Cr_2O_3	0.10(3)	n.d.	n.d.	n.d.	1.2(2)	n.d.	n.d.	n.d.	n.d.
MnO	0.01(1)	n.d.	n.d.	n.d.	n.d.	n.d.	n.d.	n.d.	n.d.
FeO*[h]	0.09(1)	0.05(4)	16.3(5)	21.7(4)	71.4(5)	6.7(5)	0.6(7)	6.8(8)	14(1)
NiO	0.08(2)	0.03(3)	n.d.	1.0(3)	n.d.	n.d.	n.d.	n.d.	n.d.
Nb_2O_5	n.d.	n.d.	n.d.	n.d.	n.d.	46(1)	n.d.	n.d.	n.d.
MoO_2	n.d.	n.d.	n.d.	74.0(6)	7.2(4)	n.d.	7.9(9)	85(1)	34(1)
Total	99.99	100.76	100.0	100.0	100.1	99.8	100.1	99.9	99.6
No. oxygen atoms	6[i]	7	4	8	4[j]				
Na	n.d.	0.00	n.d.	n.d.	n.d.				
Mg	0.45	0.19	0.67	0.32	0.06				
Al	0.90	1.57	1.93	n.d.	0.12				
Si	1.42	1.20	n.d.	n.d.	0.04				
P	n.d.	n.d.	n.d.	0.00	n.d.				
Ca	1.02	2.03	n.d.	0.07	0.06				
Ti	–	0.00	n.d.	n.d.	n.d.				
Ti^{3+}	0.05	–	–	–	–				
Ti^{4+}	0.14	–	–	–	–				
V	0.02	0.00	0.05	n.d.	0.39				
Cr	0.00	0.00	n.d.	n.d.	0.03				
Mn	0.00	0.00	n.d.	n.d.	n.d.				
Fe*	0.00	0.00	–	1.56	–				
Fe^{2+}	–	–	0.35	–	1.06				
Fe^{3+}	–	–	–	–	1.11				
Ni	0.00	n.d.	n.d.	0.07	n.d.				
Zr	n.d.	n.d.	n.d.	n.d.	n.d.				
Mo	n.d.	n.d.	n.d.	2.99	0.12				
Sum cations	4.00	5.01	3.00	5.01	3.00				

Note: Numbers in parentheses refer to the estimated standard deviation relevant to the last reported digit.
[a] Analysis contaminated by apatite.
[b] Analysis contaminated by tugarinovite.
[c] Analysis contaminated by apatite and Mo-Fe-oxide.
[d] This phase has a cubic structure, based on EBSD. Analysis contaminated by apatite and tugarinovite.
[e] Errors given inside parentheses for EPMA analyses are one standard deviation of the mean based on all of the analyses.
[f] Errors given inside parentheses for SEM-EDS analyses are one standard deviation computed from counting statistics.
[g] n.d.: not determined.
[h] All Fe as FeO.
[i] Formula computed assuming exactly 4.00 cations in a formula unit based on 6.00 oxygen atoms by adjusting cations of Ti^{3+} and Ti^{4+}.
[j] Formula computed assuming exactly 3.00 cations in a formula unit based on 4.00 oxygen atoms by adjusting cations of Fe^{2+} and Fe^{3+}.

OCCURRENCE AND ASSOCIATED MINERALS

Monipite occurs as one irregular grain, 1.3 × 2.0 μm in size (Figs. 1–2), in the central portion of an opaque assemblage (Blum et al. 1989) enclosed mostly within melilite from a fragment of a coarse-grained Ca-Al-rich inclusion, ACM-2. There are also some coarse spinel grains in contact with the opaque assemblage. The monipite crystal is approximately 1100 μm from the surface of the inclusion as defined by a Wark-Lovering rim in the plane of the section, which consists of a series of mono- and bi-mineralic layers, abutting matrix; these rims surround most coarse-grained inclusions in Allende (Fig. 1a; see Wark and Boynton 2001 and references therein). Since the Wark-Lovering rim is absent on the side closest to the monipite, we can conclude that only a portion of the original inclusion has survived. The distance to the opposite, now missing, free surface, which would also have been bounded by a Wark-Lovering rim, is unknown but we argue below that the Wark-Lovering rim shown in Figure 1a marks the free surface closest to the monipite. The surviving portion of the host inclusion is ~1400 × 2800 μm across in the plane of the type section (Fig. 1a). The observed host inclusion is melilite-rich (>90% modal melilite) with minor amounts of clinopyroxene (a solid solution between Al,Ti-diopside and grossmanite) and $MgAl_2O_4$ spinel, most of the latter residing in a band ~200 μm inboard from the Wark-Lovering rim. These features are potentially consistent with either a compact type A (CTA) inclusion, in which the mode is everywhere dominated by melilite with minor spinel and clinopyroxene, or the melilite-rich mantle portion of a type B1 inclusion. In type B1 inclusions, the melilite-rich mantle surrounds a core containing major modal clinopyroxene along with melilite, spinel, and, usually, anorthite. Since these inclusion types have significantly different bulk compositions and may have had significantly different histories (e.g., Grossman et al. 2008a), it is desirable to distinguish between these two possibilities. We, therefore, begin with a consideration of

TABLE 2. Alloys and phosphides in monipite-bearing phase assemblages

Phase	monipite	Ru-Mo-Ni alloy	Ni_2Fe alloy
Section	USNM 7554	USNM 7554	USNM 7554
Type	EPMA[a]	SEM-EDS[b]	SEM-EDS
No. analyses	3	1	1
P	16.8(2)[a]	n.d.	n.d.
Fe	1.73(7)	n.d.	32.8(0.8)
Co	1.25(5)	n.d.	n.d.
Ni	28.5(2)	14.1(8)[b]	65.9(9)
Mo	43.9(6)	29(1)	n.d.
Ru	5.2(1)	53(1)	n.d.
Rh	1.93(7)	4(1)	n.d.
Pt	n.d.[c]	n.d.	1.3(7)
Total	99.31	100.1	100.0
	Based on 1 P	Atomic %	Atomic %
P	1		
Fe	0.06	n.d.	34.23
Co	0.04	n.d.	n.d.
Ni	0.89	21.67	65.39
Mo	0.84	27.67	n.d.
Ru	0.09	47.13	n.d.
Rh	0.03	3.53	n.d.
Pt	n.d.	n.d.	0.38
Sum	2.96	100.00	100.00

[a] Errors given inside parentheses for EPMA analyses are one standard deviation of the mean based on all of the analyses.
[b] Errors given inside parentheses for SEM-EDS analyses are one standard deviation computed from counting statistics.
[c] n.d. = not determined.

the host inclusion and its petrographic type and then describe the immediate environs of the type monipite grain.

Based on multiple sections cut through the inclusion of this study, the plane of the thin section is roughly perpendicular of the surface of the original inclusion and, assuming that the inclusion was originally spherical, we estimate that it was roughly 7 mm in diameter (estimated via Fig. 1a for a chord 1380 μm across with a segment height of 260 μm). Such a large CAI would be consistent with a type B1 inclusion but unusual for CTA inclusions, which tend to be much smaller, although TS12, a CTA described by Simon et al. (1999), is 8 mm long × 1.5 mm across in section. Although a CTA is possible based on observed dimensions of the inclusion fragment sampled by USNM 7554, it is much more likely that ACM-2 is a type B1 inclusion.

The major element chemistries of melilite and spinel in ACM-2 are not diagnostic for inclusion type. Highly magnesian melilites in a melilite-rich CAI would be a signature for a type B1 inclusion but the relatively aluminous melilites observed in ACM-2 are consistent with both type B1 and CTA inclusions. The composition of clinopyroxene, however, does provide an additional clue to the identity of the host inclusion. Clinopyroxene occurring near the Wark-Lovering rim is highly titaniferous with TiO_2* (all Ti calculated as TiO_2) as high as 19 wt%. The type grossmanite crystal, which was described by Ma and Rossman (2009b), also occurs in USNM 7554 and its location is indicated in Figure 1. Grossmanites are not diagnostic for inclusion type because they are found in both CTAs and in the melilite-rich mantles of type B1 inclusions. However, clinopyroxene in the vicinity of the monipite-bearing opaque assemblage is Al,Ti-diopside, characterized by relatively modest TiO_2* contents (e.g., Table 1) ranging from 6–9 wt%. This strongly suggests that the host inclusion is a type B1 (Simon et al. 1999). It seems likely that the original inclusion broke at or near the interface between the mantle and core, a natural zone of weakness, and that the monipite-bearing section shown in Figure 1 is part of a fragment that adhered to the matrix after removal of the bulk of the inclusion.

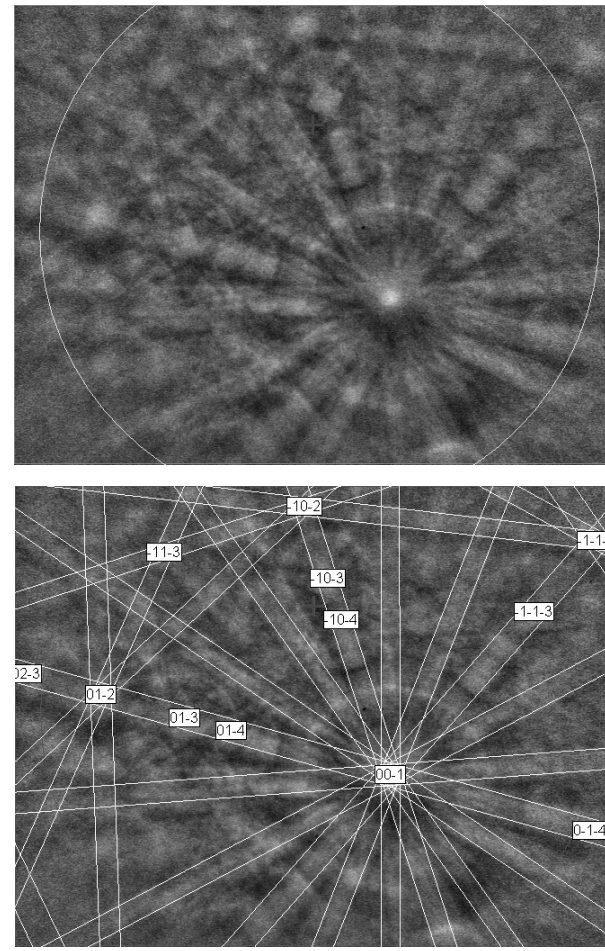

FIGURE 3. (**top**) EBSD pattern of the monipite crystal. (**bottom**) Pattern indexed using the MoNiP $P\bar{6}2m$ structure of Guérin and Sergent (1977).

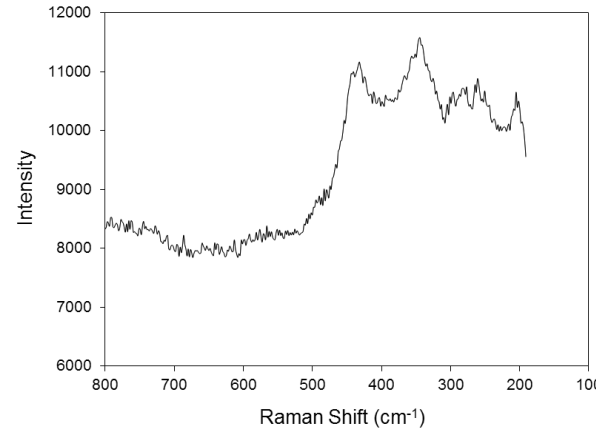

FIGURE 4. Raman spectrum of type monipite.

The monipite crystal (Fig. 2) is in contact with a Ru-Mo-Ni

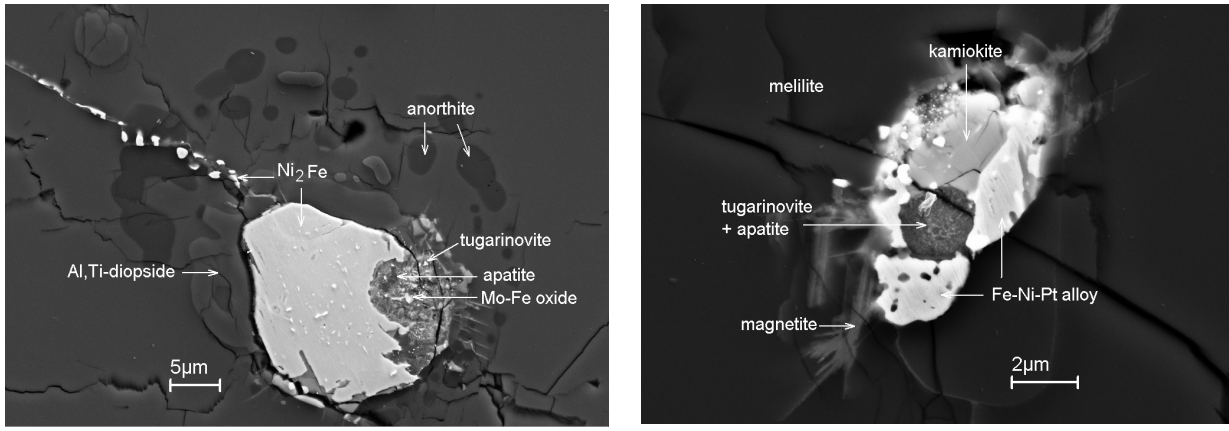

FIGURE 5. Phosphate-Mo oxide-magnetite-awaruite assemblages. (**left**) The opaque assemblage is partially enclosed by Al,Ti-diopside with a surrounding rosette of anorthite blebs, the latter most likely reflecting trapped melt. Ni-Fe alloy are scattered along a crack that extends from the opaque assemblage. (**right**) Phosphate-tugarinovite region surrounded by Pt-bearing Fe-Ni alloy and kamiokite.

metal grain ($Ru_{0.47}Mo_{0.28}Ni_{0.22}Rh_{0.04}$), which has a $P6_3/mmc$ structure based on EBSD measurements, apatite (identity confirmed via EBSD vs. merrillite), and tugarinovite (MoO_2), which also occurs partially included in the Ru-enriched alloy. A Nb-rich oxide $(Nb,V,Fe)O_2$, an unnamed cubic Mo-Fe oxide, V-Mo-bearing magnetite, kamiokite, spinel, tugarinovite, and awaruite are also present elsewhere in the opaque assemblage; compositions obtained via SEM-EDS or EPMA are given in Tables 1–2. The Nb-rich oxide has, after extracting P_2O_5 and CaO in the form of apatite, a formula of $(Nb_{0.54}V_{0.27}Fe_{0.15}Mg_{0.05}Al_{0.04})O_2$. This phase is different from the one described by Lovering et al. (1979). Their grains have much higher molar Ca/Nb (~1) and are likely to be pyrochlores, as suggested by the authors.

The monipite-Ru-Mo-Ni alloy-tugarinovite assemblage is surrounded by apatite and an asymmetric suite of partial bi- to polymineralic rings with the Nb-rich oxide $(Nb_{0.54}V_{0.27}Fe_{0.15}Mg_{0.05}Al_{0.04})O_2$ restricted to the pyroxene-spinel bounded side of the opaque assemblage and Mo-Fe oxides generally restricted to the awaruite side in Figure 2. Apatite (identity confirmed via EBSD) is found throughout the opaque assemblage in Figure 2 up to the interface with the large Ni_2Fe grain but no Ru enriched alloys are observed in this region, although they do occur as submicrometer inclusions in the large Ni_2Fe grain. Tugarinovite gives way to one or more Mo-Fe oxides with an overall molar Mo/Fe ~ 2, at least one of which is cubic (i.e., not tugarinovite or kamiokite), and kamiokite ($Fe_2^{2+}Mo_3^{4+}O_8$). Continuing left in Figure 2, these phases are largely replaced by a Mo-,V-rich magnetite. A grain of kamiokite is, however, observed at the edge of the large Ni_2Fe metal grain shown in Figures 1b and 2 and both kamiokite and Ru-Os-Mo enriched alloy grains occur as inclusions within it. Sprays of V-rich magnetite and Ni_2Fe metal extend outward from the monipite-bearing assemblage along cracks (Fig. 1b), suggesting mobility of Fe, Ni, and V.

We did not observe any additional monipite-bearing phase assemblages in 10 sections taken in series through the CAI shown in Figures 1 to 2. Molybdenite (MoS_2) is observed in one opaque assemblage with pentlandite and Pt-Ir enriched Ni-Fe alloy ($Ni_{50}Fe_{30}Pt_{17}Ir_3$), but Mo is more typically found in the form of oxides. Kamiokite is observed as inclusions in two Ni-Fe alloys; for these grains, no associated opaque assemblages were observed, although one of them had a phosphate in contact with the Ni-Fe alloy. We also encountered two opaque assemblages containing both phosphate and Mo oxides (Fig. 5). In one of these (Fig. 5a), a mixture of apatite and Mo-Fe oxide/tugarinovite forms a patch partially intruding a large grain of Ni-Fe alloy. The other example (Fig. 5b) contains a rounded cluster of tugarinovite and apatite bounded by kamiokite and a Pt-enriched Fe-Ni alloy.

Phase compositions are given in Tables 1–2. Spinel is Mg-,Al-rich but generally zoned in Fe with iron decreasing from rim to core. Clinopyroxene compositions are discussed above. Chlorine and fluorine were not detected in apatite using SEM-EDS, but we did not attempt to quantify halogen concentrations using EPMA. Apatite in an opaque assemblage from an Allende CAI described by Armstrong et al. (1985) contained 1.6 wt% Cl so it is possible that the apatite shown in Figures 1 to 2 also contains significant concentrations of Cl. To our knowledge, monipite is the first known occurrence of a phosphide in Allende, although phosphides have been reported in other CV3 chondrites such as Efremovka (Jambor et al. 2000) and NWA 6101 (Riches et al. 2010).

ORIGIN AND SIGNIFICANCE

Monipite joins allabogdanite $(Fe,Ni)_2P$, andreyivanovite (FeCrP), barringerite (Fe_2P), and florenskyite (FeTiP), as the minerals with an M_2P stoichiometry, where "M" represents a cation. Other phosphide minerals (e.g., schreibersite) have an M_3P or M_4P stoichiometry. Monipite is also the only phosphide mineral with Mo as a major component. This is also the first reported meteoritic occurrence of kamiokite and tugarinovite (and of the unnamed Nb-V and Mo-Fe oxides) in a meteorite. In this section, we briefly consider constraints on the origin of monipite. We begin with a consideration of monipite stability and general thermal history constraints derived from Type B1 inclusions, then sort out the signatures from low-temperature metasomatic processes and, finally, place monipite within the overall history of the CAI.

Monipite is readily synthesized on composition in sealed silica tubes between 800 and 1200 °C (Guérin and Sergent 1977;

Oryshchyn et al. 2001) and at high pressure (Shirotani et al. 2000) but neither high- nor low-temperature stability limits have been established. MoNiP is also known to precipitate readily in arc melted, very rapidly cooled, Mo-Pd-Ni-Cu-P glassy alloys, even at small concentrations of Mo (≤3 wt%; Ma and Inoue 2003), suggesting that MoNiP may be stable to the high temperatures encountered during melting of the host CAI. Thermodynamic and relevant high-temperature phase equilibria data are, however, lacking for monipite, so we cannot use them for a quantitative evaluation of the stability of this phase.

The high-temperature history of the host CAI would normally provide the basic framework for discussing the origin of monipite but most of the CAI is missing and we must, therefore, resort to generic constraints based on other Allende type B1 inclusions. Various textural and compositional constraints (Stolper 1982; Stolper and Paque 1986; Grossman et al. 2008b) imply maximum temperatures for type B1 inclusions of roughly 1400–1450 °C with subsequent cooling at rates of degrees to tens of degrees Celsius per hour under highly reducing conditions. Brief excursions to higher temperatures are possible but both petrographic and isotopic constraints argue against any extended residence (Stolper and Paque 1986; Richter et al. 2002). For Type B1 inclusions, formation of the melilite-rich mantle appears to have been a consequence of the volatilization of Mg and Si from near surface regions of the partially molten droplet followed by nucleation and growth of melilite in the Mg-,Si-depleted region (e.g., Mendybaev et al. 2006). Precursors to the monipite-bearing assemblage shown in Figures 1 to 2 and 5 and of other assemblages in this CAI now containing the Mo-rich phases tugarinovite and kamiokite were engulfed by melilite when the mantle crystallized. Given the highly reducing conditions during melting of the host CAI (e.g., Stolper et al. 1982; Grossman et al. 2008b), far more reducing than the Mo-MoO_2 buffer, all Mo would have been in reduced form, either in a liquid/crystalline alloy or as a phosphide (i.e., tugarinovite, kamiokite, and apatite are secondary phases). At the ~1400 °C peak temperatures of the host CAI, Fe-Ni alloys are crystalline but small amounts of C, P, or S can greatly decrease the liquidus temperature (e.g., Vogel and Horstmann 1953; Gabriel et al. 1987; Waldner and Pelton 2004). The rounded shape of most opaque assemblages in Type B inclusions suggests either brief excursions to temperatures above ~1450 °C or the inclusion of small amounts of C, P, and/or S. The monipite-bearing assemblage (Figs. 1–2) and a similar opaque assemblage observed in another section through the CAI (Fig. 5) both embay adjacent Fe-Ni alloy and are partially surrounded by spinel and Al,Ti-diopside. These objects differ from typical opaque assemblages in Allende CAIs in containing anomalously large amounts of Mo, which also decreases liquidus temperatures for Fe-Ni-rich compositions and, most importantly, P.

Allende CAIs have been altered through oxidation and vapor transport and it is important to evaluate how these secondary processes may have affected monipite and nearby phases. We take the temperature-f_{O_2} conditions for Ni_2Fe alloy-magnetite equilibrium from McMahon and Haggerty [1980; $\log f_{O_2}$ = 8.855–28 557/T(K)] and temperatures in the range of 500–800 °C as representative of this event (Armstrong et al. 1987; Blum et al. 1989). The Mo-MoO_2 buffer (O'Neill 1986) is approximately two log units more reducing than the McMahon-Haggerty conditions, so that tugarinovite (MoO_2) is the stable Mo-O phase during the alteration event, but it is several orders of magnitude more oxidizing than f_{O_2} values associated with the CAI melting event, so tugarinovite, even had it existed in a precursor, would not have survived the melting event. Tugarinovite is a secondary phase. Similar arguments can be used to assert that kamiokite is also secondary.

Large chemical potential gradients are implied by the observed phase assemblages. For example, the activity of MoO_2 is ~1 where tugarinovite is present but only 5 μm away, kamiokite contacts Ni_2Fe, for which the equilibrium can be expressed as

$$Fe_{(s)} + 3\ MoO_{2(s)} + O_{2(g)} = Fe_2Mo_3O_{8(kam)} \quad (1)$$

where "kam" refers to kamiokite. Writing an equilibrium constant expression for this reaction and solving for the activity of MoO_2 leads to

$$a_{MoO_2} = \exp\left\{\left[\frac{G^{\circ}_{\rightarrow(1)}}{RT} - \ln a_{Fe}^2 - \ln f_{O_2}\right] / 3\right\} \quad (2)$$

where we assume pure kamiokite (i.e., activity = 1). Again, using McMahon and Haggerty to determine f_{O_2} as a function of temperature with standard state data for Fe-Mo oxides from Chase et al. (1985) and Koyama et al. (2003), and activities of Fe in Fe-Ni solutions (Chuang et al. 1986), we obtain a_{MoO_2} of 0.07 (500 °C) to 0.18 (800 °C). The opaque assemblage shown in Figure 2 sustained large gradients in MoO_2 activities over just 5 μm with activities decreasing outward from the center.

The $Ru_{0.47}Mo_{0.28}Ni_{0.22}Rh_{0.04}$ alloy adjacent to monipite in Figures 1b and 2 has a $P6_3/mmc$ structure, which is the same as the element Ru, suggesting that this is a terminal Ru-rich alloy. If so, this is probably a high-temperature phase, because Ni solubility in Ru-Ni alloys is less than 10 mol% for temperatures below 900 °C, although it is possible that Mo stabilizes Ni in Ru-rich solutions. Available thermodynamic data on terminal Ru-rich alloys in the Ru-Ni and Ru-Mo binaries (Kleykamp 1989; Mazhuga et al. 1998) indicate substantial negative deviations from ideality. If the alloy equilibrated to low temperatures with contacting tugarinovite, we can write the formation reaction

$$Mo_{(s)} + O_{2(g)} = MoO_{2(tug)} \quad (3)$$

where "s" refers to the solid Ru-Mo-Ni alloy, "g" to gas, and "tug" to tugarinovite and a corresponding equilibrium constant expression, which can be rearranged to solve for the activity of Mo in the alloy:

$$a_{Mo} = \exp\left[\frac{G^{*}_{\rightarrow(3)}}{RT} - \ln f_{O_2}\right] \quad (4)$$

where $G^{*}_{\rightarrow(3)}$ is the free energy of reaction 3, and it is assumed that tugarinovite is pure MoO_2 (the small grain size of tugarinovite makes it impossible to assess purity based on the analysis given in Table 2). Taking the free energy of formation of MoO_2

from the JANAF tables (Chase et al. 1985), leads to calculated activity coefficients of 0.06 (500 °C) to 0.20 (800 °C), which reflect negative deviations from ideality, consistent with available thermodynamic data (e.g., Kleykamp 1989; Mazhuga et al. 1998). Thus, we cannot distinguish on this basis whether the Ru-Mo-Ni alloy is a relict high-temperature phase that did not equilibrate with MoO_2 or it is an alteration phase that did equilibrate with tugnarovite.

Ni, Fe, V, Mo, and P are generally viewed as being mobile during the alteration of Allende CAIs (e.g., Campbell et al. 2003; Paque et al. 2007) so that the current Mo/P of the monipite-bearing opaque assemblage, in particular, is probably not the same as it was prior to alteration. This makes specific identification of possible precursor phases difficult to establish based on major element chemistry. However, the observation of multiple occurrences of apatite, kamiokite, and tugarinovite in the host CAI, suggests that these phases represent important pathways by which metamorphism of Mo-,P-enriched precursors within this CAI was expressed. Campbell et al. (2003), for example, argued based on the PGE signature that schreibersite was originally present in the precursor to an opaque assemblage they studied in Allende but that the schreibersite was destroyed during metasomatism. In the present opaque inclusion, Mo and P concentrations in the precursor were much higher, so that monipite rather than schreibersite was the dominant phosphide and Mo concentrations were sufficiently high to support the formation of large amounts of Mo oxides.

Armstrong et al. (1985) and Bischoff and Palme (1987) described opaque assemblages from Allende CAIs that contain Mo-rich areas but these differ from the objects of this study in three important respects. First, Mo is in the form of powellite-scheelite (i.e., Ca molybdate-tungstate) rather than the Fe-Mo oxides tugarinovite and kamiokite; second, apatite is rare or absent; and, third, no phosphides are observed. These three observations are not unrelated. In the presence of large amounts of phosphide, incoming Ca vapors, probably mostly in the form of $Ca(OH)_2$ (Hashimoto 1992), reacted with P in Fe-Ni alloys and phosphides to form apatite. For monipite the overall reaction would have been

$$12MoNiP+27O_2 + 20Ca(OH)_2 = 18H_2O + 4Ca_5(PO_4)_3(OH) + 12MoO_2 + 12Ni \quad (5)$$

for the hydrated form of apatite and a similar reaction can be written for chloride transport. In the absence of significant amounts of phosphides, as is more typical of opaque assemblages (Armstrong et al. 1985; Bischoff and Palme 1987), a Ca molybdate forms in preference to the oxides tugarinovite and kamiokite. Note in Equation 5, that the molar Mo/P ratio of the product apatite + tugarinovite is 1 because the monipite source has a fixed ratio. Based on modes within the opaque assemblage shown in Figure 1b, the molar Mo/P ratio would be approximately 2. This suggests that either P was preferentially lost from the opaque assemblage relative to Mo or, perhaps more likely, that there was more Mo than P in the precursor (i.e., the precursor consisted of monipite and additional Mo-bearing phases, probably in the form of alloys).

The above considerations suggest the following basic scenario for the formation of monipite. The host CAI is the product of melting to temperatures on the order of 1400 °C, followed by cooling at degrees to tens of degrees per hour. During this melting event, Mo, P, Fe, and Ni formed immiscible metallic melts within the silicate melt of the host. During cooling, either monipite crystallized from the metallic melt (or a P-rich immiscible melt within the alloy melt), or it exsolved at lower temperatures from a Mo-P enriched crystalline alloy. At a later time, the host CAI was subjected to an alteration event that oxidized Mo and P to form apatite and Mo oxides. There are currently insufficient thermodynamic, kinetic, and phase equilibria data involving monipite to quantify the history of this phase but, if available, they could, in principle, be used to help constrain several important facets of CAI evolution including the nature of the melting event and of siderophile precursor materials and the evolution of Mo and P in CAIs both during the melting event and during later alteration.

Acknowledgments

The Caltech GPS Analytical Facility is supported, in part, by NSF grants NSF EAR-0318518 and DMR-0080065. We also acknowledge NASA grant NNG04GG14G and NSF grant EAR-0947956. We thank Alan Rubin, an anonymous reviewer, and associate editor Oliver Tschauner for helpful reviews.

References cited

Armstrong, J.T. (1995) CITZAF: A package of correction programs for the quantitative electron beam X-ray analysis of thick polished materials, thin films, and particles. Microbeam Analysis, 4, 177–200.

Armstrong, J.T., El Goresy, A., and Wasserburg, G.J. (1985) Willy: A prize noble Ur-Fremdling—Its history and implications for the formation of Fremdlinge and CAI. Geochimica et Cosmochimica Acta, 49, 1001–1022.

Armstrong, J.T., Hutcheon, I.D., and Wasserburg, G.J. (1987) Zelda and company: Petrogenesis of sulfide-rich Fremdlinge and constraints on solar nebula processes. Geochimica et Cosmochimica Acta, 51, 3155–3173.

Bischoff, A., and Palme, H. (1987) Composition and mineralogy of refractory-metal-rich assemblages from a Ca,Al-rich inclusion in the Allende meteorite. Geochimica et Cosmochimica Acta, 51, 2733–2748.

Blum, J.D., Wasserburg, G.J., Hutcheon, I.D., Beckett, J.R., and Stolper, E.M. (1989) Origin of opaque assemblages in C3V meteorites: Implications for nebular and planetary processes. Geochimica et Cosmochimica Acta, 53, 543–556.

Campbell, A.J., Simon, S.B., Humayun, M., and Grossman, L. (2003) Chemical evolution of metal in refractory inclusions in CV3 chondrites. Geochimica et Cosmochimica Acta, 67, 3119–3134.

Chase, M.W., Davies, C.A., Downey, J.R., Frurip, D.J., McDonald, R.A., and Syverud, A.N. (1985) JANAF thermochemical tables third edition. Physical and Chemical Reference Data, 14, Supplement, 1–1856.

Chuang, Y.-Y., Chang, Y.A., Schmid, R., and Lin, J.-C. (1986) Magnetic contributions to the thermodynamic functions of alloys and the phase equilibria of Fe-Ni system below 1200 K. Metallurgical Transactions, 17A, 1361–1372.

Gabriel, A., Gustafson, P., and Ansara, I. (1987) A thermodynamic evaluation of the C-Fe-Ni system. Calphad, 11, 203–218.

Grossman, L., Simon, S.B., Rai, V.K., Thiemens, M.H., Hutcheon, I.D., Williams, R.W., Galy, A., Ding, T., Fedkin, A.V., Clayton, R.N., and Mayeda, T.K. (2008a) Primordial compositions of refractory inclusions. Geochimica et Cosmochimica Acta, 72, 3001–3021.

Grossman, L., Beckett, J.R., Fedkin, A.V., Simon, S.B., and Ciesla, F.J. (2008b) Redox conditions in the solar nebula: Observational, experimental, and theoretical constraints. In G.J. MacPherson, D.W. Mittlefehldt, J.H. Jones, and S.B. Simon, Eds., Oxygen in the Solar System, 68, p. 93–140. Reviews in Mineralogy & Geochemistry, Mineralogical Society of America, Chantilly, Virginia.

Guérin, P.R., and Sergent, M. (1977) Structure Cristalline de NiMoP. Acta Crystallographica B, 33, 2820–2823.

Hashimoto, A. (1992) The effect of H_2O gas on volatilities of planet-forming major elements: I. Experimental determination of thermodynamic properties of Ca-, Al-, and Si-hydroxide gas molecules and its application to the solar nebula. Geochimica et Cosmochimica Acta, 56, 511–532.

Jambor, J.L., Kovalenker, V.A., and Roberts, A.C. (2000) New mineral names. American Mineralogist, 85, 873–877.

Kleykamp, H. (1989) Constitution and thermodynamics of the Mo-Ru, Mo-Pd, Ru-Pd and Mo-Ru-Pd systems. Journal of Nuclear Materials, 167, 49–63.

Koyama, K., Morishita, M., Harada, T., and Maekawa, N. (2003) Determination of standard Gibbs energies of formation of $Fe_2Mo_3O_{12}$, $Fe_2Mo_3O_8$, Fe_2MoO_4, and $FeMoO_4$ of the Fe-Mo-O ternary system and μ phase of the Fe-Mo binary

system by electromotive force measurement using a Y_2O_3-stabilized ZrO_2 solid electrolyte. Metallurgical and Materials Transactions, 34B, 653–659.
Lovering, J.F., Wark, D.A., and Sewell, D.K.B. (1979) Refractory oxide, titanite, niobate and silicate accessory mineralogy of some type B Ca-Al-rich inclusions in the Allende meteorite. Lunar and Planetary Science, 10, 745–747.
Ma, C. (2010) Hibonite-(Fe), $(Fe,Mg)Al_{12}O_{19}$, a new alteration mineral from the Allende meteorite. American Mineralogist, 95, 188–191.
Ma, C., and Inoue, A. (2003) Microstructure and mechanical properties of Cr, Mo, Fe, Ta modified Pd-Ni-Cu-P glassy alloys prepared by copper-mold casting. Materials Transactions, 44, 188–196.
Ma, C., and Rossman, G.R. (2008) Barioperovskite, $BaTiO_3$, a new mineral from the Benitoite Mine, California. American Mineralogist, 93, 154–157.
——— (2009a) Tistarite, Ti_2O_3, a new refractory mineral from the Allende meteorite. American Mineralogist, 94, 841–844.
——— (2009b) Grossmanite, $CaTi^{3+}AlSiO_6$, a new pyroxene from the Allende meteorite. American Mineralogist, 94, 1491–1494.
Ma, C., Beckett, J.R., and Rossman, G.R. (2009a) Discovery of a new phosphide mineral, monipite (MoNiP), in an Allende type B1 CAI. Meteoritics & Planetary Science, 44, A127.
——— (2009b) Allendeite and hexamolybdenum: two new ultra-refractory minerals in Allende and two missing links. Lunar and Planetary Science Conference 40, Abstract no. 1402.
Mazhuga, T.G., Danilenko, V.M., Velikanova, T.Ya., and Semenova, E.L. (1998) Thermodynamic calculation of phase equilibria in the Ti-Ru, Ti-Os, Ni-Ru binary systems. Calphad, 22, 59–67.
McMahon, B.M., and Haggerty, S.E. (1980) Experimental studies bearing on the magnetite-alloy-sulfide association in the Allende meteorite: Constraints on the conditions of chondrule formation. Proceedings of the Lunar and Planetary Science Conference, 11, 1003–1025.
Mendybaev, R.A., Richter, F.M., and Davis, A.M. (2006) Crystallization of melilite from CMAS-liquids and the formation of the melilite mantle of Type B1 CAIs: Experimental simulations. Geochimica et Cosmochimica Acta, 70, 2622–2642.
Nagai, M., Fukiage, T., and Kurata, S. (2005) Hydrodesulfurization of dibenzothiopene over alumina-supported nickel molybdenum phosphide catalysts. Catalysis Today, 106, 201–205.
O'Neill, H.St.C. (1986) Mo-MoO_2 (MOM) oxygen buffer and the free energy of formation of MoO_2. American Mineralogist, 71, 1007–1010.
Oryshchyn, S.V., Le Sénéchal, C., Députier, S., Bauer, J., Guérin, R., and Akselrud, L.G. (2001) New ternary phases in the Mo-Ni-P system: Synthesis and crystal structures. Journal of Solid State Chemistry, 160, 156–166.
Paque, J.M., Burnett, D.S., and Beckett, J.R. (2007) Zoning patterns of Fe and V in spinel from a type B Ca-Al-rich inclusion: Constraints on subsolidus thermal history. Meteoritics & Planetary Science, 42, 899–912.
Pouchou, J.-L., and Pichoir, F. (1991) Quantitative analysis of homogeneous or stratified microvolumes applying the model "PAP". In K.F.J. Heinrich and D.E. Newbury, Eds., Electron Probe Quantitation, p. 31–75. Plenum Press, New York.
Riches, A.J.V., Liu, Y., Zhang, A., and Taylor, L.A. (2010) Description of newly-identified CV3 chondrites: Salient textural and mineralogical characteristics. Lunar and Planetary Science 41, Abstract no. 2561.
Richter, F.M., Davis, A.M., Ebel, D.S., and Hashimoto, A. (2002) Elemental and isotopic fractionation of Type B calcium-, aluminum-rich inclusions: Experiments, theoretical considerations, and constraints on their evolution. Geochimica et Cosmochimica Acta, 66, 521–540.
Shirotani, I., Takaya, M., Kaneko, I., Sekine, C., and Yagi, T. (2000) Superconductivity of MRuP and MNiP (M = Mo or W) prepared at high pressure. Solid State Communications, 116, 683–686.
Simon, S.B., Davis, A.M., and Grossman, L. (1999) Origin of compact type A refractory inclusions from CV3 carbonaceous chondrites. Geochimica et Cosmochimica Acta, 63, 1233–1248.
Stolper, E. (1982) Crystallization sequences of Ca-Al-rich inclusions from Allende: An experimental study. Geochimica et Cosmochimica Acta, 46, 2159–2180.
Stolper, E., and Paque, J.M. (1986) Crystallization sequences of Ca-Al-rich inclusions from Allende: The effects of cooling rate and maximum temperature. Geochimica et Cosmochimica Acta, 50, 1785–1806.
Stolper, E., Paque, J., and Rossman, G.R. (1982) The influence of oxygen fugacity and cooling rate on the crystallization of Ca-Al-rich inclusions from Allende. Lunar and Planetary Science, 13, 772–773.
Sun, F., Wu, W., Wu, Z., Guo, J., Wei, Z., Yang, Y., Jiang, Z., Tian, F., and Li, C. (2004) Dibenzothiopene hydrosulfurization activity and surface sites of silica-supported MoP, Ni_2P, and Ni-Mo-P catalysts. Journal of Catalysis, 228, 298–310.
Vogel, R., and Horstmann, D. (1953) Das Zustandsschaubild Eisen-Eisenphosphid-Molybdänphosphid-Molybdän. Archiv für das Eisenhüttenwesen, 24, 369–374.
Waldner, P., and Pelton, A.D. (2004) Critical thermodynamic assessment and modeling of the Fe-Ni-S system. Metallurgical and Materials Transactions, 35B, 897–907.
Wark, D.A., and Boynton, W.V. (2001) The formation of rims on calcium-aluminum-rich inclusions: Step I—Flash heating. Meteoritics & Planetary Science, 36, 1135–1166.

Manuscript received February 21, 2013
Manuscript accepted August 31, 2013
Manuscript handled by Oliver Tschauner